Applied Ocean Research 31 (2009) 101–110

Contents lists available at ScienceDirect

Applied Ocean Research

journal homepage: www.elsevier.com/locate/apor

Interaction of water waves with vertical cylinders using null-field integral equations

Jeng-Tzong Chen [a,b,*], Ying-Te Lee [a], Yi-Jhou Lin [a]

[a] Department of Harbor and River Engineering, National Taiwan Ocean University, Keelung, Taiwan
[b] Department of Mechanical and Mechatronics Engineering, National Taiwan Ocean University, Keelung, Taiwan

ARTICLE INFO

Article history:
Received 6 October 2008
Received in revised form
18 June 2009
Accepted 19 June 2009
Available online 19 July 2009

Keywords:
Null-field integral equation
Degenerate kernel
Fourier series
Helmholtz equation
Water wave
Scattering

ABSTRACT

The scattering of water waves by bottom-mounted vertical circular cylinders is solved by using the null-field integral equations in conjunction with degenerate kernels and Fourier series to avoid calculating the Cauchy and Hadamard principal values. In the implementation, the null-field point can be exactly located on the real boundary owing to the introduction of degenerate kernels for fundamental solutions. An adaptive observer system of polar coordinates is considered to fully employ the properties of degenerate kernels. For the hypersingular equation, vector decomposition for the radial and tangential gradients is carefully considered. This method can be seen as a semi-analytical approach since errors attribute from the truncation of Fourier series. Neither hypersingularity in the Burton and Miller approach nor the CHIEF concept was required to deal with the problem of irregular frequencies. Five advantages of free of calculating principal value, well-posed algebraic system, convergence rate of exponential order, meshfree and elimination of boundary-layer effect, are achieved by using the present approach. Numerical results are given for the forces and free-surface elevation around the circular boundaries. Also, the near-trapped behavior arisen from the physical resonance is detected. A general-purpose program for water wave impinging several circular cylinders with arbitrary number, radii, and positions was developed. Several examples of water wave structure interaction by vertical circular cylinders were demonstrated to see the validity of the present formulation.

1. Introduction

For designing the offshore platforms mounted on the sea bed, it is important to understand the interaction between the vertical cylinders and plane wave. There is considerable interest in this topic among countries with long coasts, e.g., USA, Japan and Taiwan. For the problem of plane waves impinging vertical cylinders, a closed-form solution of force on a single vertical cylinder was derived by MacCamy and Fuchs [1]. A similar analysis extended to two cylinders was investigated by Spring and Monkmeyer [2]. They used the addition theorem to analytically derive the scattered-wave solution. Not only equal size but also unequal size of the cylinders subject to the incident wave of arbitrary angle was analyzed. They claimed that their method is a direct approach, since they formulated the problem by using a linear algebraic system and the solution is obtained easily from a single matrix inversion. A different method presented by Twersky [3] is called the multiple-scattering approach. In his approach, he took one cylinder at a time and the scattering coefficient was solved sequentially. Besides, the boundary conditions which they solved are also different. One is the Neumann-type boundary condition and the other is the Dirichlet-type boundary condition. Chakrabarti [4] extended the work of Spring and Monkmeyer to solve a complex matrix. In his work, he saved a half computer storage space. Based on the work of Simon [5], McIver and Evans [6] proposed an approximate solution based on the assumption that the cylinders are widely spaced. Later, in the work of Linton and Evans [7], they also used the same approximate method as that proposed earlier by Spring and Monkmeyer. The main contribution was to provide a simple formula for the potential on the surfaces of the cylinders which made the computation of forces much more straightforward. However, their results for four cylinders [7] were incorrect and a corrigendum was given in [8]. Nevertheless, it still deviated slightly from those obtained by using the collocation boundary element method as proposed by Perrey-Debain et al. [9].

In the Fredholm integral equations, the degenerate kernel plays an important role. However, its applications in practical problems seem to have taken a back seat to other methods. This method can be seen as one kind of approximation method, and the kernel

* Corresponding author. Tel.: +886 2 24622192x6177; fax: +886 2 24632375.
E-mail address: jtchen@mail.ntou.edu.tw (J.-T. Chen).

0141-1187/$ – see front matter © 2009 Elsevier Ltd. All rights reserved.
doi:10.1016/j.apor.2009.06.004

function is expressed as finite sums of products by two linearly independent functions as follows:

$$K(x,s) = \sum_{k=1}^{n} A_k(x)B_k(s). \tag{1}$$

Sometimes, the degenerate kernel is called separable kernel since the source and field points are separated. This terminology is not coined by the authors, but follows the literature [10–12]. The concept of generating "optimal" degenerate kernels has been proposed by Sloan et al. [13]. They also proved to it to be equivalent to the iterated Petrov–Galerkin approximation. Later, Kress [14] proved that the integral equations of the second kind in conjunction with degenerate kernels have the convergence rate of exponential order instead of the linear algebraic order. The convergence rate is better than that of the conventional BEM. In the literature, it is observed that exact solutions for boundary value problems are only limited for simple cases. Therefore, proposing a semi-analytical approach for solving BVP with circular boundaries of various numbers, positions and radii is our goal in this article.

It seems that the present formulation is more complex than the method proposed by Linton and Evans for researchers who are not familiar with boundary integral equation method. The Linton and Evans method can be seen as an improved Trefftz method [15,16] (or the so-called multipole Trefftz method) for the problem with multiply-connected domain. The method of Linton and Evans is an analytical approach but the solution is not exact or closed-form since the unknown coefficients can not be obtained in an explicit form. Although the solution representation of the Linton and Evans method is simpler than our approach, the convergence behavior is pointwise for the strong solution. However, the convergence behavior of our approach is superior to that of the Linton and Evans method. For the boundary integral solution, it converges to L_2 energy sense in an exponential order. It is noted that we can deal with other shape of cross section in our approach, if the degenerate kernels corresponding to the special geometry are available. For example, degenerate kernel for the ellipse can be found in the book of Morse and Feshbach [17]. Also, the work of the elliptic case using the method of Linton and Evans is given in Martin's book [18], and the numerical results are implemented by Chatjigeorgiou and Mavrakos [19]. On the other hand, some formulae are not found in the mathematical handbook or were not derived by mathematicians for the special geometry. That is to say, we have a challenging work in deriving the degenerate kernel for a special geometry case. Besides, our approach can be applied to problems containing both circular and elliptic cylinders since we introduce adaptive coordinate and vector decomposition. For the Linton and Evans approach, it may have difficulty to implement since the addition theorem for translating the polar coordinates to the elliptic coordinates and vice versa is not available to the authors' best knowledge. Simply speaking, the addition theorem is not available to transform Bessel to Mathieu functions when a problem contains circle and ellipse together.

For the problems of multiple cylinders, Martin as well as Linton and Evans have proposed an analytical model to deal with these problems. Since double summations due to the use of the addition theorem are contained in the solution representation, the numerical implementation is sometimes not computer-friendly due to ill-posedness of the Bessel function. For the problems with two close-cylinders, a larger number of series terms are required to ensure the accuracy. However, ill-posed behavior in double summations may deteriorate the numerical solution. Martin [10] also addressed this point in his book (p. 132) as quoted follows: "Linton and Evans found that taking $M = 6$ gave result accurate to four significant figures, except when the cylinders were very close together". Based on collocation technique of the null-field BIEM, no difficulty occurs since we use the addition theorem only one series sum in conjunction with adaptive coordinate and vector decomposition. Two advantages of our approach are summarized below: A higher number of series terms to simulate a close-cylinders problem can be implemented in real computations. Also, our approach can deal with a problem containing circular and elliptic cylinders at the same time. A comparison table between the Linton and Evans method and the present approach is given in Table 1.

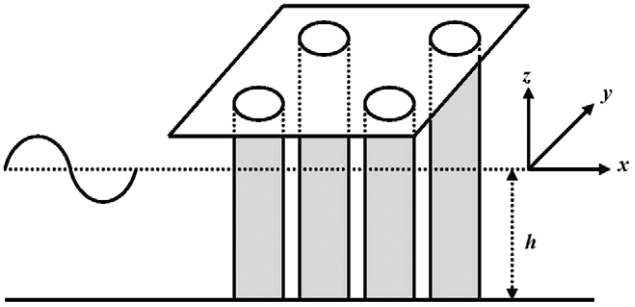

Fig. 1. Problem statement of water waves with an array of vertical cylinders.

In this paper, the null-field boundary integral equation method (BIEM) is employed to solve the scattering problems of water wave across an array of circular cylinders. To fully utilize the geometry of circular boundary, not only Fourier series for boundary densities as previously used by many researchers but also the degenerate kernel for fundamental solutions in the present formulation is incorporated into the null-field integral equation. All the improper boundary integrals are free of calculating the principal values (Cauchy and Hadamard) in place of series sum. In order to analytically integrate each circular boundary for the null-field equation, the adaptive observer system of polar coordinate is considered to fully employ the property of degenerate kernel. To avoid double integration in the Galerkin sense, point collocation approach is considered. Free of worrying how to choose the collocation points, uniform collocation along the circular boundary yields a well-posed matrix. For the hypersingular equation, vector decomposition for the radial and tangential gradients is carefully considered, especially for the eccentric case. Trapped modes are also examined. Finally, problems of water wave structure interaction by arbitrary number of vertical circular cylinders mounted on the sea bed are solved to demonstrate the validity of the present method.

2. Problem statement and integral formulation

2.1. Problem statement

Now we assume N vertical cylinders mounted at $z = -h$ upward to the free surface as shown in Fig. 1. The governing equation of the water wave problem is the Laplace equation

$$\nabla^2 \Phi(x,y,z;t) = 0, \quad (x,y,z) \in D, \tag{2}$$

where ∇^2 and D are the Laplacian operator and the domain of interest, respectively, and $\Phi(x,y,z;t)$ is the velocity potential which satisfies the boundary conditions of sea bed, kinematic and dynamic boundary conditions at free surface as shown below:

$$-\frac{\partial \Phi}{\partial n} = 0, \qquad z = -h(x,y), \tag{3}$$

$$-\Phi_z = H_t - \Phi_x H_x - \Phi_y H_y, \quad z = H(x,y,t), \tag{4}$$

$$-\Phi_t + gz + \frac{1}{2}(\Phi_x^2 + \Phi_y^2 + \Phi_z^2) = B(t), \quad z = H(x,y,t), \tag{5}$$

Table 1
Comparison of the present approach and the Linton and Evans method.

	Present approach (BIE)	Method of Linton and Evans
Formulation	Green's third identity	Potential superposition
Solution representation	Integral representation $u(x)=\int_B T(s,x)u(s)\mathrm{d}B(s)-\int_B U(s,x)t(s)\mathrm{d}B(s)$	Trefftz series solution $u(r,\theta)=\sum_{j=1}^{N}\sum_{n=-\infty}^{\infty}A_n^j\frac{J_n'(ka_j)}{H_n'(ka_j)}H_n(kr_j)\mathrm{e}^{\mathrm{i}n\theta_j}$
Unknown coefficients	Fourier coefficient	Weighting A_n^j
Addition theorem	$H_0(kr)$	$H_m(k\rho)\mathrm{e}^{\mathrm{i}m\phi}$, $m=0,1,2,\ldots$
Linear algebraic system	$[B]\{x\}=\{c\}$	$[\bar{B}]\{A_n^j\}=\{\bar{c}\}$
Extension to general geometry containing circle and ellipse	Yes	No
Domain type	Interior and exterior	Exterior only
Solution behavior	Weak	Strong
Convergent behavior	L_2 energy sense in an exponential order	Pointwise

in which g is the gravity acceleration, $H(x,y,t)$ is the free-surface elevation and $B(t)$ is the Bernoulli constant. Based on the linear water wave theory and using the technique of separation variable for space and time, we have

$$\Phi(x,y,z;t)=\mathrm{Re}\{\phi(x,y)f(z)\mathrm{e}^{-\mathrm{i}\omega t}\} \tag{6}$$

where

$$f(z)=\frac{-\mathrm{i}gA}{\omega}\frac{\cosh k(z+h)}{\cosh kh} \tag{7}$$

in which ω is the angular frequency, k represents the wavenumber, $H(x,y,t)$ can be defined by

$$H(x,y,t)=\mathrm{Re}\{\eta(x,y)\mathrm{e}^{-\mathrm{i}\omega t}\} \tag{8}$$

where

$$\eta(x,y)=Au(x,y) \tag{9}$$

and A represents the amplitude of incident wave of angle β as shown below:

$$u_I(x,y)=\mathrm{e}^{\mathrm{i}k(x\cos\beta+y\sin\beta)}\equiv\mathrm{e}^{\mathrm{i}kr\cos(\theta-\beta)}. \tag{10}$$

Substituting Eq. (6) into Eq. (2), we have

$$(\nabla^2+k^2)u(x,y)=0,\quad (x,y)\in D. \tag{11}$$

Rigid cylinders yield the Neumann boundary conditions as shown below:

$$\frac{\partial u(x,y)}{\partial n}=0,\quad (x,y)\in B. \tag{12}$$

The dispersion relationship is

$$k\tanh kh=\frac{\omega^2}{g}. \tag{13}$$

The dynamic pressure can be obtained by

$$p=-\rho_0\frac{\partial\Phi}{\partial t}=\rho_0 gA\frac{\cosh k(z+h)}{\cosh kh}u(x,y)\mathrm{e}^{-\mathrm{i}\omega t}, \tag{14}$$

where ρ_0 denotes the density. The two components of the first-order force X^j on the jth cylinder are given by integrating the pressure over the circular boundary as shown below:

$$X^j=-\frac{\rho gAa_j}{k}\tanh kh\int_0^{2\pi}u(x,y)\begin{Bmatrix}\cos\theta_j\\ \sin\theta_j\end{Bmatrix}\mathrm{d}\theta_j, \tag{15}$$

where a_j denotes the radius of the jth cylinder.

2.2. Dual null-field integral equations — the conventional version

The integral equation for the domain point can be derived from Green's third identity [20], we have

$$2\pi u(x)=\int_B T(s,x)\,u(s)\,\mathrm{d}B(s)-\int_B U(s,x)\,t(s)\,\mathrm{d}B(s),\quad x\in D, \tag{16}$$

$$2\pi t(x)=\int_B M(s,x)\,u(s)\,\mathrm{d}B(s)-\int_B L(s,x)\,t(s)\,\mathrm{d}B(s),\quad x\in D, \tag{17}$$

where s and x are the source and field points, respectively, D is the domain of interest, $t(s)=\frac{\partial u(s)}{\partial n_s}$, n_s and n_x denote the outward normal vectors at the source point s and field point x, respectively. The kernel function, $U(s,x)=-\frac{\pi i}{2}H_0^{(1)}(kr)$, is the fundamental solution which satisfies

$$\nabla^2U(s,x)=2\pi\delta(x-s) \tag{18}$$

where $\delta(x-s)$ denotes the Dirac-delta function, $H_n^{(1)}(kr)=J_n(kr)+\mathrm{i}Y_n(kr)$ is the nth order Hankel function of the first kind, J_n is the nth order Bessel function of the first kind, Y_n is the nth order Bessel function of the second kind, $r=|x-s|$, $\mathrm{i}^2=-1$. The other kernel functions, $T(s,x)$, $L(s,x)$, and $M(s,x)$, are defined by

$$T(s,x)=\frac{\partial U(s,x)}{\partial n_s}, \tag{19}$$

$$L(s,x)=\frac{\partial U(s,x)}{\partial n_x}, \tag{20}$$

$$M(s,x)=\frac{\partial^2U(s,x)}{\partial n_s\partial n_x}. \tag{21}$$

By moving the field point to the boundary, Eqs. (16) and (17) reduce to

$$\pi u(x)=C.P.V.\int_B T(s,x)\,u(s)\,\mathrm{d}B(s)-R.P.V.\int_B U(s,x)\,t(s)\,\mathrm{d}B(s),\quad x\in B, \tag{22}$$

$$\pi t(x)=H.P.V.\int_B M(s,x)\,u(s)\,\mathrm{d}B(s)-C.P.V.\int_B L(s,x)\,t(s)\,\mathrm{d}B(s),\quad x\in B, \tag{23}$$

where $R.P.V.$, $C.P.V.$ and $H.P.V.$ denote the Riemann principal value (Riemann sum), the Cauchy principal value and the Hadamard principal value (or Hadamard finite part), respectively. Once the field point x locates outside the domain ($x\in D^c$), we obtain the dual null-field integral equations as shown below

$$0=\int_B T(s,x)\,u(s)\,\mathrm{d}B(s)-\int_B U(s,x)\,t(s)\,\mathrm{d}B(s),\quad x\in D^c, \tag{24}$$

$$0=\int_B M(s,x)\,u(s)\,\mathrm{d}B(s)-\int_B L(s,x)\,t(s)\,\mathrm{d}B(s),\quad x\in D^c, \tag{25}$$

where D^c is the complementary domain. Eqs. (16), (17), (24) and (25) are conventional formulations where the point can not be

located on the real boundary. Singularity occurs and concept of principal values is required once Eqs. (22) and (23) are considered. The flux $t(s)$ is the directional derivative of $u(s)$ along the outer normal direction at s. For the interior point, $t(x)$ is artificially defined. For example, $t(x) = \partial u(s)/\partial x_1$, if $\mathbf{n} = (1, 0)$ and $t(x) = \partial u(x)/\partial x_2$, if $\mathbf{n} = (0, 1)$ where (x_1, x_2) is the Cartensian coordinates of the field point x.

2.3. Dual boundary integral formulation — the present version

By introducing the degenerate kernels, the collocation point can be located on the real boundary free of facing principal value using bump contours. Therefore, the representations of integral equations including the boundary point for the interior problem can be written as

$$2\pi u(x) = \int_B T^I(s,x)u(s)\mathrm{d}B(s) - \int_B U^I(s,x)t(s)\mathrm{d}B(s), \quad x \in D \cup B, \tag{26}$$

$$2\pi t(x) = \int_B M^I(s,x)u(s)\mathrm{d}B(s) - \int_B L^I(s,x)t(s)\mathrm{d}B(s), \quad x \in D \cup B, \tag{27}$$

and

$$0 = \int_B T^E(s,x)u(s)\mathrm{d}B(s) - \int_B U^E(s,x)t(s)\mathrm{d}B(s), \quad x \in D^c \cup B, \tag{28}$$

$$0 = \int_B M^E(s,x)u(s)\mathrm{d}B(s) - \int_B L^E(s,x)t(s)\mathrm{d}B(s), \quad x \in D^c \cup B, \tag{29}$$

once the kernels are expressed in terms of appropriate degenerate forms (denoted by the subscripts I and E) instead of the closed-form fundamental solution without distinction. It is noted that x in Eqs. (26)–(29) can exactly be located on the real boundary. For the exterior problem, the domain of interest is in the external region of the circular boundary and the complementary domain is in the internal region of the circle. Therefore, the null-field integral equations are represented as

$$2\pi u(x) = \int_B T^E(s,x)u(s)\mathrm{d}B(s) - \int_B U^E(s,x)t(s)\mathrm{d}B(s), \quad x \in D \cup B, \tag{30}$$

$$2\pi t(x) = \int_B M^E(s,x)u(s)\mathrm{d}B(s) - \int_B L^E(s,x)t(s)\mathrm{d}B(s), \quad x \in D \cup B, \tag{31}$$

and

$$0 = \int_B T^I(s,x)u(s)\mathrm{d}B(s) - \int_B U^I(s,x)t(s)\mathrm{d}B(s), \quad x \in D^c \cup B, \tag{32}$$

$$0 = \int_B M^I(s,x)u(s)\mathrm{d}B(s) - \int_B L^I(s,x)t(s)\mathrm{d}B(s), \quad x \in D^c \cup B. \tag{33}$$

Also, x in Eqs. (30)–(33) can exactly be located on the real boundary. For various problems (interior or exterior), we used different kernel functions (denoted by superscripts "I" and "E") so that jump behavior across the boundary can be captured. Therefore, different expressions of the kernels for the interior and exterior observer points are used and they will be elaborated on latter.

2.4. Expansions of fundamental solution and boundary density

Based on the separable property, the kernel function $U(s,x)$ can be expanded into degenerate form by separating the source point and field point in the polar coordinates. Since degenerate kernels can describe the fundamental solutions in two regions (interior and exterior domains), the BIEs for the domain point of Eqs. (26)–(27) and Eqs. (30)–(31) and null-field BIEs of Eqs. (28)–(29) and Eqs. (32)–(33) can be directly employed for the boundary point. In the real implementation, the null-field point can be exactly pushed on the real boundary since we introduce the expression of degenerate kernel for fundamental solutions. By using the polar coordinates, we can express $x = (\rho, \phi)$ and $s = (R, \theta)$. The four kernels U, T, L and M can be expressed in terms of degenerate kernels as shown below [21]:

$$U(s,x) = \begin{cases} U^I(R,\theta;\rho,\phi) = \dfrac{-\pi\mathrm{i}}{2}\displaystyle\sum_{m=0}^{\infty}\varepsilon_m J_m(k\rho)H_m^{(1)}(kR) \\ \quad \times \cos(m(\theta-\phi)), \quad R \geq \rho, \\ U^E(R,\theta;\rho,\phi) = \dfrac{-\pi\mathrm{i}}{2}\displaystyle\sum_{m=0}^{\infty}\varepsilon_m H_m^{(1)}(k\rho)J_m(kR) \\ \quad \times \cos(m(\theta-\phi)), \quad R < \rho, \end{cases} \tag{34}$$

$$T(s,x) = \begin{cases} T^I(R,\theta;\rho,\phi) = \dfrac{-\pi k\mathrm{i}}{2}\displaystyle\sum_{m=0}^{\infty}\varepsilon_m J_m(k\rho)H_m^{\prime(1)}(kR) \\ \quad \times \cos(m(\theta-\phi)), \quad R > \rho, \\ T^E(R,\theta;\rho,\phi) = \dfrac{-\pi k\mathrm{i}}{2}\displaystyle\sum_{m=0}^{\infty}\varepsilon_m H_m^{(1)}(k\rho)J_m'(kR) \\ \quad \times \cos(m(\theta-\phi)), \quad R < \rho, \end{cases} \tag{35}$$

$$L(s,x) = \begin{cases} L^I(R,\theta;\rho,\phi) = \dfrac{-\pi k\mathrm{i}}{2}\displaystyle\sum_{m=0}^{\infty}\varepsilon_m J_m'(k\rho)H_m^{(1)}(kR) \\ \quad \times \cos(m(\theta-\phi)), \quad R > \rho, \\ L^E(R,\theta;\rho,\phi) = \dfrac{-\pi k\mathrm{i}}{2}\displaystyle\sum_{m=0}^{\infty}\varepsilon_m H_m^{\prime(1)}(k\rho)J_m(kR) \\ \quad \times \cos(m(\theta-\phi)), \quad R < \rho, \end{cases} \tag{36}$$

$$M(s,x) = \begin{cases} M^I(R,\theta;\rho,\phi) = \dfrac{-\pi k^2\mathrm{i}}{2}\displaystyle\sum_{m=0}^{\infty}\varepsilon_m J_m'(k\rho)H_m^{\prime(1)}(kR) \\ \quad \times \cos(m(\theta-\phi)), \quad R \geq \rho, \\ M^E(R,\theta;\rho,\phi) = \dfrac{-\pi k^2\mathrm{i}}{2}\displaystyle\sum_{m=0}^{\infty}\varepsilon_m H_m^{\prime(1)}(k\rho)J_m'(kR) \\ \quad \times \cos(m(\theta-\phi)), \quad R < \rho, \end{cases} \tag{37}$$

where ε_m is the Neumann factor

$$\varepsilon_m = \begin{cases} 1, & m = 0, \\ 2, & m = 1, 2, \ldots, \infty. \end{cases} \tag{38}$$

Eqs. (34)–(37) can be seen as the subtraction theorem instead of the addition theorem since we care $|x - s|$ not $|x + s|$. Mathematically speaking, the expressions of fundamental solutions in Eqs. (34)–(37) are termed degenerate kernels (or separable kernels) which can expand the kernel to sums of products of function of the field point x alone and function of the source point s alone. If the finite sum of series is considered, the kernel is finite rank. As we shall see in the later sections, the theory of boundary integral equations with degenerate kernel is nothing more than the linear algebra. Since the potentials resulted from $T(s,x)$ and $L(s,x)$ are discontinuous across the boundary, the potentials of $T(s,x)$ and $L(s,x)$ for $R \to \rho^+$ and $R \to \rho^-$ are different. This is the reason why $R = \rho$ is not included in the expression for the degenerate kernels of $T(s,x)$ and $L(s,x)$ in Eqs. (35) and (36). The

degenerate kernels simply serve as the means to evaluate regular integrals analytically and take the limits analytically. The reason is that integral equation for the domain point of Eq. (26) and null-field integral equation of Eq. (28) yield the same algebraic equation when the limit is taken from the inside or from the outside of the region. Both limits represent the same algebraic equation that is an approximate counterpart of the boundary integral equation, that for the case of a smooth boundary has in the left-hand side term $\pi u(x)$ or $\pi t(x)$ rather than $2\pi u(x)$ or $2\pi t(x)$ for the domain point or 0 for the point outside the domain. Besides, the limiting case to the boundary is also addressed. The continuous and jump behavior across the boundary is well captured by the Wronskian property of Bessel function J_m and Y_m bases

$$W(J_m(kR), Y_m(kR)) = Y'_m(kR)J_m(kR) - Y_m(kR)J'_m(kR) = \frac{2}{\pi kR}, \tag{39}$$

as shown below

$$\int_0^{2\pi} \left(T^I(s,x) - T^E(s,x)\right)\cos(m\theta)R\mathrm{d}\theta = 2\pi\cos(m\phi), \quad x \in B, \tag{40}$$

$$\int_0^{2\pi} \left(T^I(s,x) - T^E(s,x)\right)\sin(m\theta)R\mathrm{d}\theta = 2\pi\sin(m\phi), \quad x \in B. \tag{41}$$

After employing Eqs. (40) and (41), Eqs. (30) and (32) yield the same linear algebraic equation when x is exactly pushed on the boundary from the domain or the complementary domain. A proof for the Laplace case can be found [22].

In order to fully utilize the geometry of circular boundary, the potential $u(s)$ and its normal flux $t(s)$ can be approximated by employing the Fourier series. Therefore, we obtain

$$u(s) = a_0 + \sum_{n=1}^{\infty}(a_n\cos n\theta + b_n\sin n\theta), \tag{42}$$

$$t(s) = p_0 + \sum_{n=1}^{\infty}(p_n\cos n\theta + q_n\sin n\theta), \tag{43}$$

where a_0, a_n, b_n, p_0, p_n and q_n are the Fourier coefficients and θ is the polar angle which is equally discretized. Eqs. (32) and (33) can be easily calculated by employing the orthogonal property of Fourier series. In the real computation, only the finite P terms are used in the summation of Eqs. (42) and (43).

2.5. Adaptive observer system

Since the boundary integral equations are frame indifferent, *i.e.* rule of objectivity is obeyed. Adaptive observer system is chosen to fully employ the property of degenerate kernels. Fig. 2 shows the boundary integration for the circular boundaries. It is worthy of noting that the origin of the observer system can be adaptively located on the center of the corresponding circle under integration to fully utilize the geometry of circular boundary. The dummy variable in the integration on the circular boundary is just the angle (θ) instead of the radial coordinate (R). By using the adaptive observer system, all the boundary integrals can be determined analytically free of principal value.

2.6. Vector decomposition technique for the potential gradient in the hypersingular formulation

Since hypersingular equation plays an important role for dealing with fictitious frequencies, potential gradient of the field quantity is required to calculate. For the eccentric case, the field point and source point may not locate on the circular boundaries

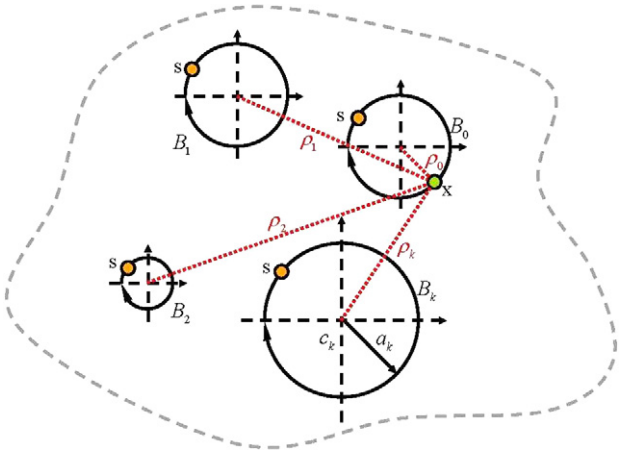

Fig. 2. The adaptive observer system.

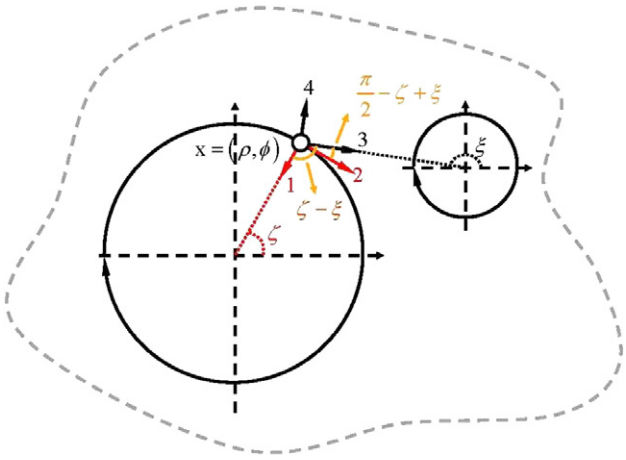

Fig. 3. Vector decomposition technique for the potential gradient in the hypersingular equation.

with the same center except the two points on the same circular boundary or on the annular cases. Special treatment for the normal derivative should be taken care. As shown in Fig. 3 where the origins of observer system are different, the true normal direction $\hat{e}_1$ with respect to the collocation point x on the B_j boundary should be superimposed by using the radial direction $\hat{e}_3$ and angular direction $\hat{e}_4$. We call this treatment "vector decomposition technique". According to the concept, Eqs. (36) and (37) can be modified as

$$L(s,x) = \begin{cases} L^I(s,x) = \dfrac{-\pi ki}{2}\displaystyle\sum_{m=0}^{\infty}\varepsilon_m J'_m(k\rho)H_m^{(1)}(kR) \\ \quad \times \cos(m(\theta-\phi))\cos(\zeta-\xi) \\ \quad -\dfrac{\pi mi}{2\rho}\displaystyle\sum_{m=0}^{\infty}\varepsilon_m J_m(k\rho)H_m^{(1)}(kR) \\ \quad \times \sin(m(\theta-\phi))\sin(\zeta-\xi), \quad R>\rho, \\ L^E(s,x) = \dfrac{-\pi ki}{2}\displaystyle\sum_{m=0}^{\infty}\varepsilon_m H_m^{\prime(1)}(k\rho)J_m(kR) \\ \quad \times \cos(m(\theta-\phi))\cos(\zeta-\xi) \\ \quad -\dfrac{\pi mi}{2\rho}\displaystyle\sum_{m=0}^{\infty}\varepsilon_m H_m^{(1)}(k\rho)J_m(kR) \\ \quad \times \sin(m(\theta-\phi))\sin(\zeta-\xi), \quad R<\rho, \end{cases} \tag{44}$$

$$M(s,x)=\begin{cases} M^I(s,x)=\dfrac{-\pi k^2\mathrm{i}}{2}\displaystyle\sum_{m=0}^{\infty}\varepsilon_m J'_m(k\rho)H'^{(1)}_m(kR) \\ \quad\times\cos(m(\theta-\phi))\cos(\zeta-\xi) \\ \quad-\dfrac{\pi mki}{2\rho}\displaystyle\sum_{m=0}^{\infty}\varepsilon_m J_m(k\rho)H'^{(1)}_m(kR) \\ \quad\times\sin(m(\theta-\phi))\sin(\zeta-\xi), \quad R\geq\rho, \\ M^E(s,x)=\dfrac{-\pi k^2\mathrm{i}}{2}\displaystyle\sum_{m=0}^{\infty}\varepsilon_m H'^{(1)}_m(k\rho)J'_m(kR) \\ \quad\times\cos(m(\theta-\phi))\cos(\zeta-\xi) \\ \quad-\dfrac{\pi mki}{2\rho}\displaystyle\sum_{m=0}^{\infty}\varepsilon_m H^{(1)}_m(k\rho)J'_m(kR) \\ \quad\times\sin(m(\theta-\phi))\sin(\zeta-\xi), \quad R<\rho, \end{cases} \tag{45}$$

2.7. Linear algebraic equation

In order to calculate the $2P+1$ unknown Fourier coefficients, $2P+1$ boundary points on each circular boundary are needed to be collocated. By collocating the null-field point exactly on the kth circular boundary for Eqs. (32) and (33) as shown in Fig. 2, we have

$$0=\sum_{j=1}^{N}\int_{B_j}T^E(\mathbf{s},\mathbf{x}_k)u(\mathbf{s})\mathrm{d}B(\mathbf{s})-\sum_{j=1}^{N}\int_{B_j}U^E(\mathbf{s},\mathbf{x}_k)t(\mathbf{s})\mathrm{d}B(\mathbf{s}),\quad \mathbf{x}_k\in D^c\cup B, \tag{46}$$

$$0=\sum_{j=1}^{N}\int_{B_j}M^E(\mathbf{s},\mathbf{x}_k)u(\mathbf{s})\mathrm{d}B(\mathbf{s})-\sum_{j=1}^{N}\int_{B_j}L^E(\mathbf{s},\mathbf{x}_k)t(\mathbf{s})\mathrm{d}B(\mathbf{s}),\quad \mathbf{x}_k\in D^c\cup B, \tag{47}$$

where N is the number of circles. It is noted that the path is anticlockwise for the outer circle. Otherwise, it is clockwise. For the B_j integral of the circular boundary, the kernels of $U(s,x)$, $T(s,x)$, $L(s,x)$ and $M(s,x)$ are respectively expressed in terms of degenerate kernels of Eqs. (34), (35), (44) and (45) with respect to the observer origin at the center of B_j. The boundary densities of $u(s)$ and $t(s)$ are substituted by using the Fourier series of Eqs. (42) and (43), respectively. In the B_j integration, we set the origin of the observer system to collocate at the center c_j of B_j to fully utilize the degenerate kernel and Fourier series. By moving the null-field point exactly on the real boundary B_k from outside of the domain D^C in the numerical implementation, a linear algebraic system is obtained

$$[\mathbf{U}]\{\mathbf{t}\}=[\mathbf{T}]\{\mathbf{u}\}, \tag{48}$$

$$[\mathbf{L}]\{\mathbf{t}\}=[\mathbf{M}]\{\mathbf{u}\}, \tag{49}$$

where $[\mathbf{U}]$, $[\mathbf{T}]$, $[\mathbf{L}]$ and $[\mathbf{M}]$ are the influence matrices with a dimension of $N\times(2P+1)$ by $N\times(2P+1)$, $\{\mathbf{t}\}$ and $\{\mathbf{u}\}$ denote the vectors for $t(s)$ and $u(s)$ of the Fourier coefficients with a dimension of $N\times(2P+1)$ by 1, in which, $[\mathbf{U}]$, $[\mathbf{T}]$, $[\mathbf{L}]$, $[\mathbf{M}]$, $\{\mathbf{u}\}$ and $\{\mathbf{t}\}$ are defined as follows:

$$[\mathbf{U}]=[\mathbf{U}_{\alpha\beta}]=\begin{bmatrix}\mathbf{U}_{11}&\mathbf{U}_{12}&\cdots&\mathbf{U}_{1N}\\ \mathbf{U}_{21}&\mathbf{U}_{22}&\cdots&\mathbf{U}_{2N}\\ \vdots&\vdots&\ddots&\vdots\\ \mathbf{U}_{N1}&\mathbf{U}_{N2}&\cdots&\mathbf{U}_{NN}\end{bmatrix}, \tag{50}$$

$$[\mathbf{T}]=[\mathbf{T}_{\alpha\beta}]=\begin{bmatrix}\mathbf{T}_{11}&\mathbf{T}_{12}&\cdots&\mathbf{T}_{1N}\\ \mathbf{T}_{21}&\mathbf{T}_{22}&\cdots&\mathbf{T}_{2N}\\ \vdots&\vdots&\ddots&\vdots\\ \mathbf{T}_{N1}&\mathbf{T}_{N2}&\cdots&\mathbf{T}_{NN}\end{bmatrix}, \tag{51}$$

$$[\mathbf{L}]=[\mathbf{L}_{\alpha\beta}]=\begin{bmatrix}\mathbf{L}_{11}&\mathbf{L}_{12}&\cdots&\mathbf{L}_{1N}\\ \mathbf{L}_{21}&\mathbf{L}_{22}&\cdots&\mathbf{L}_{2N}\\ \vdots&\vdots&\ddots&\vdots\\ \mathbf{L}_{N1}&\mathbf{L}_{N2}&\cdots&\mathbf{L}_{NN}\end{bmatrix}, \tag{52}$$

$$[\mathbf{M}]=[\mathbf{M}_{\alpha\beta}]=\begin{bmatrix}\mathbf{M}_{11}&\mathbf{M}_{12}&\cdots&\mathbf{M}_{1N}\\ \mathbf{M}_{21}&\mathbf{M}_{22}&\cdots&\mathbf{M}_{2N}\\ \vdots&\vdots&\ddots&\vdots\\ \mathbf{M}_{N1}&\mathbf{M}_{N2}&\cdots&\mathbf{M}_{NN}\end{bmatrix}, \tag{53}$$

$$\{\mathbf{u}\}=\begin{Bmatrix}\mathbf{u}_1\\ \mathbf{u}_2\\ \vdots\\ \mathbf{u}_N\end{Bmatrix},\qquad \{\mathbf{t}\}=\begin{Bmatrix}\mathbf{t}_1\\ \mathbf{t}_2\\ \vdots\\ \mathbf{t}_N\end{Bmatrix}, \tag{54}$$

where the vectors $\{\mathbf{u}_k\}$ and $\{\mathbf{t}_k\}$ are in the form of $\{a_0^k\ a_1^k\ b_1^k\cdots\ a_p^k\ b_p^k\}^T$ and $\{p_0^k\ p_1^k\ q_1^k\cdots\ p_p^k\ q_p^k\}^T$; the first subscript "$\alpha$" ($\alpha=1,2,\ldots,N$) in the $[\mathbf{U}_{\alpha\beta}]$ denotes the index of the αth circle where the collocation point is located and the second subscript "β" ($\beta=1,2,\ldots,N$) denotes the index of the βth circle where the boundary data $\{\mathbf{u}_k\}$ or $\{\mathbf{t}_k\}$ are routed. The number of circular holes is N and the highest harmonic of truncated terms is P. The coefficient matrix of the linear algebraic system is partitioned into blocks, and each diagonal block ($\mathbf{U}_{pp}$) corresponds to the influence matrices due to the same circle of collocation and Fourier expansion. After uniformly collocating points along the αth circular boundary, the sub-matrix can be written as given in Box I.

It is noted that the superscript "0s" in the first equation in Box I disappears since $\sin(0\theta)=0$, and the element of $[\mathbf{U}_{\alpha\beta}]$, $[\mathbf{T}_{\alpha\beta}]$, $[\mathbf{L}_{\alpha\beta}]$ and $[\mathbf{M}_{\alpha\beta}]$ are defined as

$$U^{nc}=\int_{B_k}U(s_k,x_m)\cos(n\theta_k)R_k\mathrm{d}\theta_k, \tag{55}$$

$$U^{ns}=\int_{B_k}U(s_k,x_m)\sin(n\theta_k)R_k\mathrm{d}\theta_k, \tag{56}$$

$$T^{nc}=\int_{B_k}T(s_k,x_m)\cos(n\theta_k)R_k\mathrm{d}\theta_k, \tag{57}$$

$$T^{ns}=\int_{B_k}T(s_k,x_m)\sin(n\theta_k)R_k\mathrm{d}\theta_k, \tag{58}$$

$$L^{nc}=\int_{B_k}L(s_k,x_m)\cos(n\theta_k)R_k\mathrm{d}\theta_k, \tag{59}$$

$$L^{ns}=\int_{B_k}L(s_k,x_m)\sin(n\theta_k)R_k\mathrm{d}\theta_k, \tag{60}$$

$$M^{nc}=\int_{B_k}M(s_k,x_m)\cos(n\theta_k)R_k\mathrm{d}\theta_k, \tag{61}$$

$$M^{ns}=\int_{B_k}M(s_k,x_m)\sin(n\theta_k)R_k\mathrm{d}\theta_k, \tag{62}$$

where $n=1,2,\ldots,P$, $\phi_m(n=1,2,\ldots,2P+1)$ is the polar angle of the collocating point $\mathbf{x}_m$ along the boundary. After obtaining the unknown Fourier coefficients, the origin of observer system is set to c_j in the B_j integration as shown in Fig. 4 to obtain the interior potential by employing Eq. (30). The flowchart of the present method is shown in Fig. 5.

3. Illustrative examples

For the third example, we consider water wave structure problem by an array of four bottom-mounted vertical rigid circular cylinders with the same radius a located at the vertices of a square $(-b,-b)$, $(b,-b)$, (b,b), $(-b,b)$, respectively, as shown

$$[\mathbf{U}_{\alpha\beta}] = \begin{bmatrix} U^{0c}_{\alpha\beta}(\phi_1) & U^{1c}_{\alpha\beta}(\phi_1) & U^{1s}_{\alpha\beta}(\phi_1) & \cdots & U^{Pc}_{\alpha\beta}(\phi_1) & U^{Ps}_{\alpha\beta}(\phi_1) \\ U^{0c}_{\alpha\beta}(\phi_2) & U^{1c}_{\alpha\beta}(\phi_2) & U^{1s}_{\alpha\beta}(\phi_2) & \cdots & U^{Pc}_{\alpha\beta}(\phi_2) & U^{Ps}_{\alpha\beta}(\phi_2) \\ U^{0c}_{\alpha\beta}(\phi_3) & U^{1c}_{\alpha\beta}(\phi_3) & U^{1s}_{\alpha\beta}(\phi_3) & \cdots & U^{Pc}_{\alpha\beta}(\phi_3) & U^{Ps}_{\alpha\beta}(\phi_3) \\ \vdots & \vdots & \vdots & \ddots & \vdots & \vdots \\ U^{0c}_{\alpha\beta}(\phi_{2P}) & U^{1c}_{\alpha\beta}(\phi_{2P}) & U^{1s}_{\alpha\beta}(\phi_{2P}) & \cdots & U^{Pc}_{\alpha\beta}(\phi_{2P}) & U^{Ps}_{\alpha\beta}(\phi_{2P}) \\ U^{0c}_{\alpha\beta}(\phi_{2P+1}) & U^{1c}_{\alpha\beta}(\phi_{2P+1}) & U^{1s}_{\alpha\beta}(\phi_{2P+1}) & \cdots & U^{Pc}_{\alpha\beta}(\phi_{2P+1}) & U^{Ps}_{\alpha\beta}(\phi_{2P+1}) \end{bmatrix}$$

$$[\mathbf{T}_{\alpha\beta}] = \begin{bmatrix} T^{0c}_{\alpha\beta}(\phi_1) & T^{1c}_{\alpha\beta}(\phi_1) & T^{1s}_{\alpha\beta}(\phi_1) & \cdots & T^{Pc}_{\alpha\beta}(\phi_1) & T^{Ps}_{\alpha\beta}(\phi_1) \\ T^{0c}_{\alpha\beta}(\phi_2) & T^{1c}_{\alpha\beta}(\phi_2) & T^{1s}_{\alpha\beta}(\phi_2) & \cdots & T^{Pc}_{\alpha\beta}(\phi_2) & T^{Ps}_{\alpha\beta}(\phi_2) \\ T^{0c}_{\alpha\beta}(\phi_3) & T^{1c}_{\alpha\beta}(\phi_3) & T^{1s}_{\alpha\beta}(\phi_3) & \cdots & T^{Pc}_{\alpha\beta}(\phi_3) & T^{Ps}_{\alpha\beta}(\phi_3) \\ \vdots & \vdots & \vdots & \ddots & \vdots & \vdots \\ T^{0c}_{\alpha\beta}(\phi_{2P}) & T^{1c}_{\alpha\beta}(\phi_{2P}) & T^{1s}_{\alpha\beta}(\phi_{2P}) & \cdots & T^{Pc}_{\alpha\beta}(\phi_{2P}) & T^{Ps}_{\alpha\beta}(\phi_{2P}) \\ T^{0c}_{\alpha\beta}(\phi_{2P+1}) & T^{1c}_{\alpha\beta}(\phi_{2P+1}) & T^{1s}_{\alpha\beta}(\phi_{2P+1}) & \cdots & T^{Pc}_{\alpha\beta}(\phi_{2P+1}) & T^{Ps}_{\alpha\beta}(\phi_{2P+1}) \end{bmatrix}$$

$$[\mathbf{L}_{\alpha\beta}] = \begin{bmatrix} L^{0c}_{\alpha\beta}(\phi_1) & L^{1c}_{\alpha\beta}(\phi_1) & L^{1s}_{\alpha\beta}(\phi_1) & \cdots & L^{Pc}_{\alpha\beta}(\phi_1) & L^{Ps}_{\alpha\beta}(\phi_1) \\ L^{0c}_{\alpha\beta}(\phi_2) & L^{1c}_{\alpha\beta}(\phi_2) & L^{1s}_{\alpha\beta}(\phi_2) & \cdots & L^{Pc}_{\alpha\beta}(\phi_2) & L^{Ps}_{\alpha\beta}(\phi_2) \\ L^{0c}_{\alpha\beta}(\phi_3) & L^{1c}_{\alpha\beta}(\phi_3) & L^{1s}_{\alpha\beta}(\phi_3) & \cdots & L^{Pc}_{\alpha\beta}(\phi_3) & L^{Ps}_{\alpha\beta}(\phi_3) \\ \vdots & \vdots & \vdots & \ddots & \vdots & \vdots \\ L^{0c}_{\alpha\beta}(\phi_{2P}) & L^{1c}_{\alpha\beta}(\phi_{2P}) & L^{1s}_{\alpha\beta}(\phi_{2P}) & \cdots & L^{Pc}_{\alpha\beta}(\phi_{2P}) & L^{Ps}_{\alpha\beta}(\phi_{2P}) \\ L^{0c}_{\alpha\beta}(\phi_{2P+1}) & L^{1c}_{\alpha\beta}(\phi_{2P+1}) & L^{1s}_{\alpha\beta}(\phi_{2P+1}) & \cdots & L^{Pc}_{\alpha\beta}(\phi_{2P+1}) & L^{Ps}_{\alpha\beta}(\phi_{2P+1}) \end{bmatrix}$$

$$[\mathbf{M}_{\alpha\beta}] = \begin{bmatrix} M^{0c}_{\alpha\beta}(\phi_1) & M^{1c}_{\alpha\beta}(\phi_1) & M^{1s}_{\alpha\beta}(\phi_1) & \cdots & M^{Pc}_{\alpha\beta}(\phi_1) & M^{Ps}_{\alpha\beta}(\phi_1) \\ M^{0c}_{\alpha\beta}(\phi_2) & M^{1c}_{\alpha\beta}(\phi_2) & M^{1s}_{\alpha\beta}(\phi_2) & \cdots & M^{Pc}_{\alpha\beta}(\phi_2) & M^{Ps}_{\alpha\beta}(\phi_2) \\ M^{0c}_{\alpha\beta}(\phi_3) & M^{1c}_{\alpha\beta}(\phi_3) & M^{1s}_{\alpha\beta}(\phi_3) & \cdots & M^{Pc}_{\alpha\beta}(\phi_3) & M^{Ps}_{\alpha\beta}(\phi_3) \\ \vdots & \vdots & \vdots & \ddots & \vdots & \vdots \\ M^{0c}_{\alpha\beta}(\phi_{2P}) & M^{1c}_{\alpha\beta}(\phi_{2P}) & M^{1s}_{\alpha\beta}(\phi_{2P}) & \cdots & M^{Pc}_{\alpha\beta}(\phi_{2P}) & M^{Ps}_{\alpha\beta}(\phi_{2P}) \\ M^{0c}_{\alpha\beta}(\phi_{2P+1}) & M^{1c}_{\alpha\beta}(\phi_{2P+1}) & M^{1s}_{\alpha\beta}(\phi_{2P+1}) & \cdots & M^{Pc}_{\alpha\beta}(\phi_{2P+1}) & M^{Ps}_{\alpha\beta}(\phi_{2P+1}) \end{bmatrix}$$

Box I.

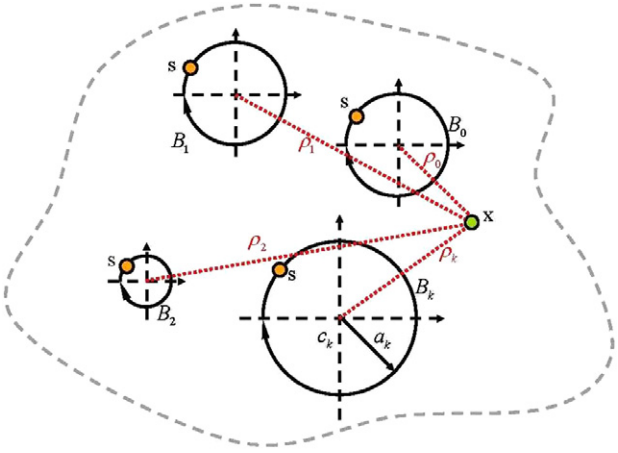

Fig. 4. Sketch of the boundary integral equation for the domain point.

in Fig. 6. By considering the incident wave in the direction of 45 degrees, the first-order force for four cylinders in the direction of the incident wave determined by Perrey-Debain et al. and the result of the present method are shown in Fig. 7. It is found that the force effect on cylinder 2 and cylinder 4 is identical as expected due to symmetry. After comparing with the result of Perrey-Debain et al. [9], good agreement is made. The maximum free-surface elevation amplitude is plotted in Fig. 8. It agrees well with that of the plane wave BEM by Perrey-Debain et al. [9]. However, the results of our approach and Perrey-Debain et al. do not agree well with those of Linton and Evans [8]. Nevertheless, the potentials at the north pole of each cylinder are compared well with the BEM data given by Perrey- et al. [9] as shown in Table 2. We also used the four north poles to test the convergence behavior as shown in Fig. 9. It is found the results converge very fast. Eight number of truncation terms (P) is adopted to have the accuracy of five figures. It may be noted that in Table 2 the results of Linton & Evans and Perrey-Derbain et al. agree to within 8 or 9 significant figures, while the present results agree to within 5 or 6 figures. For the numerical viewpoint, the different codes of the Bessel and Hankel functions may be used in both sides, Perrey-Debain et al. and our group. We could not confirm that which one is better. The main difference may stem from the package of Bessel and Hankel functions. The two agreeable results to 8 or 9 significant figures were both provided by Perrey-Debain et al. from their computer system and software. If we implement the Linton and Evans method, we also obtain agreeable results after comparing with our data using the BIEM. However, the relative error of our approach is much less than 0.5%. The result is acceptable from the engineering point of view.

For detecting the near-trapped behavior, we changed the ratio of a/b to 0.8. It means that the four cylinders are close to each

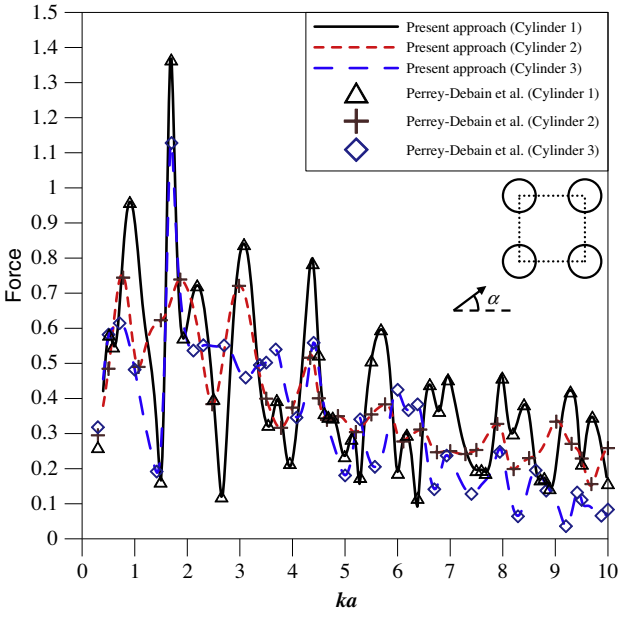

Fig. 7. The first-order force for four cylinders by using the proposed method.

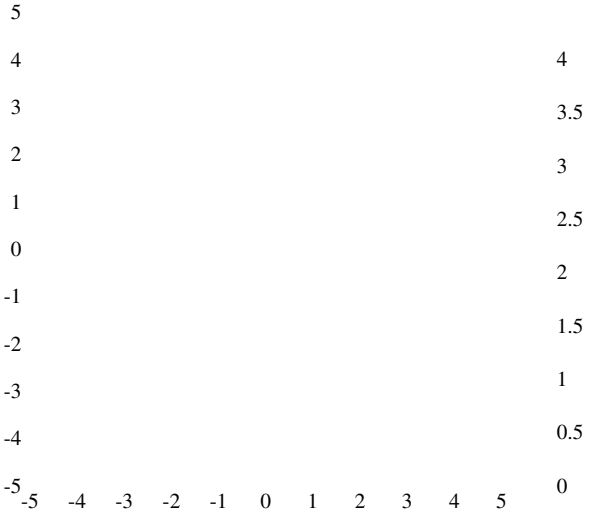

Fig. 8. Contour of the maximum free-surface elevation amplitude.

Fig. 5. Flowchart of the present method.

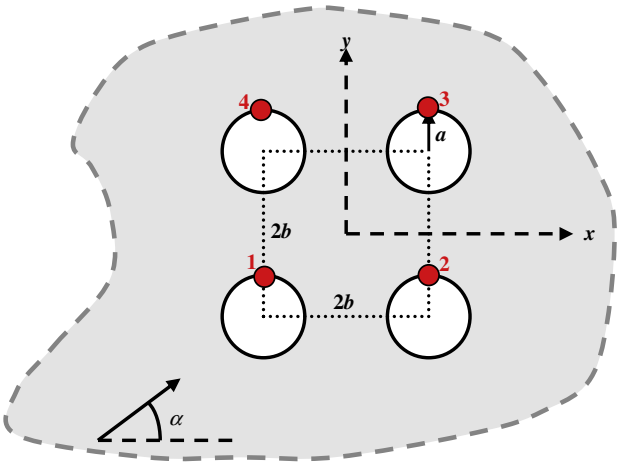

Fig. 6. Interaction of an incident water wave with four cylinders.

other. Fig. 10 shows the forces in the direction of wave advance versus the wavenumber (ka). It can be found that the peak force on cylinders 1 and 3 is about 54 times force of an isolated cylinder at the wavenumber $ka = 4.08482$. This phenomenon is the physical resonance. We also found that peak does not appear on cylinders 2 and 4. After comparing with the work of Evans and Porter [23] which was implemented by using the Linton and Evans formula [7], Fig. 10 shows good agreements on cylinders 1 and 3. However, some deviations are found on cylinders 2 and 4.

In this example, we agree that the method of Linton and Evans is an analytical approach but the solution is not exact or closed-form since the unknown coefficients must be determined by a linear algebraic equation. We also used the Linton and Evans result to verify the validity of our approach. However, the results are not consistent. Although Linton and Evans have corrected once in [8], they pointed out that their figure is incorrect owing to insufficient points being used to represent them. However, some incorrect results still exist. When ka is in the range of 1.5 to 2.0 in Fig. 7, the forces in the direction of wave advance on cylinders 1 and 3 are very similar to the results of Linton and Evans, but the force on cylinder 2 is different from their result (cylinder 1 in [8]). Fortunately, we found that the result of Perrey-Debain et al. [9] by using plane wave BEM and our results match. We may wonder that the points they used are still insufficient.